Dielectrometry Measurements of Moisture Dynamics in Oil-impregnated Pressboard

Y. Sheiretov and M. Zahn

Massachusetts Institute of Technology,
Laboratory for Electromagnetic and
Electronic Systems, Cambridge, MA

ABSTRACT

The complex dielectric spectrum of pressboard is a function of its moisture content and temperature. In oil-impregnated pressboard of medium and low humidity the dielectric spectrum's shape and amplitude do not change with variations in temperature and moisture content, but only shift in frequency. Thus it is possible to create a 'universal' curve, with appropriate temperature correction factors, which can be used to extract information about the moisture dynamics of solid transformer insulation from dielectrometry measurements. To create the universal curve, measurements are taken with the material placed in a parallel-plate structure whose complex impedance is measured. To measure spatial distributions of dielectric properties, imposed ω-k (frequency-wavenumber) dielectrometry is used, where a set of interdigitated electrodes on one surface of the material cause the electric field to have a limited depth of penetration into the dielectric, proportional to the electrode spacing. Measurements using the parallel-plate methodology establish a mapping of the dielectric spectrum of EHV-Weidmann HIVAL pressboard impregnated with Shell Diala A$^{\text{TM}}$ transformer oil, as a function of temperature and water content. This mapping is then used to determine spatial moisture profiles in pressboard in other experiments which make use of a three-wavelength interdigitated sensor.

1. INTRODUCTION

1.1. MOTIVATION

IN this paper we continue earlier dielectrometry research applied to moisture dynamics of solid and liquid transformer insulation [1–4].

The presence of moisture in the solid (pressboard) and liquid (oil) transformer insulation, is a major factor that affects the operation of power transformers. Although moisture does not seem to greatly affect the conductivity of the oil, it can reduce its dielectric strength [5]. Moisture also affects the conductivity of the pressboard, which in turn increases the dissipated power and the rate of static charge relaxation, which may be a crucial factor in static electrification phenomena [6].

Load transients which transformers undergo, especially upon power-up, cause rapid changes in the insulation's temperature. Temperature affects the solubility equilibrium of moisture between the solid and liquid insulation and also directly influences the insulation's conductivity [7]. Moisture in the oil may under fast decreasing temperature transients result in free water that can lead to electrical breakdown. A mass transfer process of water

results from the equilibrium imbalance, in which at higher temperatures moisture leaves the pressboard to enter the oil. The oil initially establishes moisture equilibrium with an interfacial zone at the surface of the pressboard. The steady state is reached when moisture from deep inside the pressboard diffuses to the surface to establish a uniform moisture distribution. The transient interfacial dry zones are highly insulating, and as a consequence significant surface charge may accumulate to cause surface spark discharges.

The dielectrometry methods developed specifically for pressboard have applications in many other fields also. The dielectric properties of a material are greatly affected by many of its other physical properties, such as temperature, pressure, mechanical stress, etc. In polymers, the permittivity may be related to the degree of polymerization. There are many applications in quality control, where deviations in the dielectric properties of a material may correspond to flaws in its structure.

As materials age, their permittivity and conductivity may change too. In general, whenever the condition of a dielectric material must be monitored, dielectrometry measurements provide a simple, non-destructive, real-time measurement, which can be related to the property in question.

1.2. DIELECTRIC PROPERTIES OF MATERIALS

There are two parameters of a medium that determine the quasi-static distribution of electric fields: the dielectric permittivity ε and the conductivity σ. If a system is under ac steady-state operation, every quantity $F(t)$ may be expressed as the real part of a complex quantity varying at radian frequency ω

$$F(x, y, z, t) = \Re\left\{ \widehat{F}(x, y, z)e^{i\omega t} \right\} \qquad (1)$$

If ε and σ are constant with time, we may write the total current density as a sum of displacement and conduction current densities. In terms of complex amplitudes

$$\widehat{J} = \widehat{J_d} + \widehat{J_c} = i\omega\varepsilon\widehat{E} + \sigma\widehat{E}$$
$$= i\omega\widehat{E}\left(\varepsilon + \frac{\sigma}{i\omega}\right) = i\omega\varepsilon^*\widehat{E} \qquad (2)$$

where $\varepsilon^* = (\varepsilon - i\sigma/\omega)$ is the complex permittivity.

The dielectric spectrum of a material is a representation of its complex permittivity, $\varepsilon^* = \varepsilon' - i\varepsilon''$, as a function of frequency. The real component $\varepsilon' = \varepsilon$ gives the permittivity while the imaginary component $\varepsilon'' = \sigma/\omega$ determines the power dissipation (loss) in the material.

In an ohmic material, ε and σ are independent of the frequency or amplitude of the applied electric field, and

a plot of $\log(\varepsilon''/\varepsilon_0)$ vs. $\log\omega$ has a slope of -1. In a dispersive material, when ε'' is plotted against frequency on a log-log scale, it can be characterized by one or more loss peaks. The magnitude of the slope at which these peaks are approached on either side is between 0 and 1 for most materials [8]. For every loss peak in the ε'' spectrum, there is an associated elevation in the ε' spectrum proportional to the area under the corresponding peak in ε'', as required by the Kramers-Kronig relations [8].

1.3. MOISTURE DYNAMIC PROCESSES IN PRESSBOARD/OIL SYSTEMS

During thermal transients complex dynamic processes occur as temperature gradients develop. Temperature transients disturb the moisture equilibrium of the system, causing the initiation of moisture mass transfer processes. Transformer oil and pressboard are very dissimilar materials, in that the former is hydrophobic and the latter is hydrophilic. Typical values for the water content of pressboard are 0.5 to 5%, while in oil at room temperature the saturation moisture content is ~ 50 ppm (parts per million) [9, 10]. As a consequence, almost all of the moisture present in the system resides in the pressboard. As the temperature changes moisture will move into or out of the pressboard via diffusion.

The rate of diffusion of moisture through the oil and the pressboard determines the time rates of change of the moisture distribution, and thus how long it takes before equilibrium is reached. Earlier experiments have determined the diffusion constants of water in these two media to have the values shown in Table 1 [4].

Table 1.
Diffusion coefficients of water in transformer oil and pressboard [4].

Diffusion coeff.	in oil	in pressboard
Symbol	D_o	D_p
Value at 15°C	1.3×10^{-11}	6.7×10^{-14}
Value at 70°C	1.1×10^{-10}	6.0×10^{-12}

In order to appreciate the magnitude of these diffusion constants, we can calculate that the diffusion times of water across $\Delta = 1$ mm of pressboard, given by $\tau = \Delta^2/D_p$ are half a year and two days at 15 and 70°C, respectively. What this means is that equilibrium is generally never reached in an operating transformer, given how quickly the oil temperature changes with the power load and the ambient air temperature. Instead, oil equilibrates only with a thin layer of pressboard at its surface. This implies that the surface of the pressboard can become extremely dry, causing a highly insulating surface that may lead to static charge accumulation and partial discharges, and ultimately catastrophic failure.

The equilibrium of moisture between the oil and the pressboard is what determines the direction of the mass transfer processes in the pressboard/oil system. This equilibrium is extremely sensitive to temperature. This is how a temperature transient drives the system out of equilibrium and initiates the mass transfer processes. If, for example, the moisture concentration in the paper is 0.5%, at 20°C, the oil humidity in equilibrium with it is ~ 0.5 ppm. If the oil temperature then changes to 80°C, the new equilibrium value for the oil humidity becomes close to 6.5 ppm, *i.e.* thirteen times higher, which would drive water out of the pressboard surface and leave it very dry until moisture deep in the pressboard diffuses to the surface on a time scale of order τ.

1.4. SCOPE OF THIS WORK

We present the following distinct steps in our work:

1. Use the parallel-plate sensor to develop the 'universal' spectrum of oil-impregnated pressboard as a function of moisture and temperature.

2. Use the three-wavelength sensor to measure transient moisture distributions.

3. Develop efficient parameter estimation algorithms to interpret data collected with the three-wavelength sensor

The results and methods presented are preliminary, aimed at developing experimental and numerical methods that show the promise of this technique. More research is needed to refine these methods and to collect more complete data on the materials in question.

2. FEATURES OF THE DIELECTRIC SPECTRUM OF PRESSBOARD

2.1. PARALLEL PLATE SENSOR

The simplest way to measure the permittivity and the conductivity of a material is to place it between a pair of parallel plates of known area and separation. This test cell can be modeled as a resistor in parallel with a capacitor. The complex admittance of the structure can be measured, and from there its permittivity and conductivity can be calculated.

We have used this simple idea in the development of the parallel-plate sensor, whose structure is shown in Figure 1. The capacitive structure is comprised of the driven electrode and the sensing electrode. Underneath the sensing electrode lies the guard electrode. The guard electrode is driven by a buffer amplifier stage to be always at the same potential as the sensing electrode. The sensing electrode is also surrounded by a ring electrode, which is connected to the guard electrode. In addition to shielding the sensing electrode from external electric
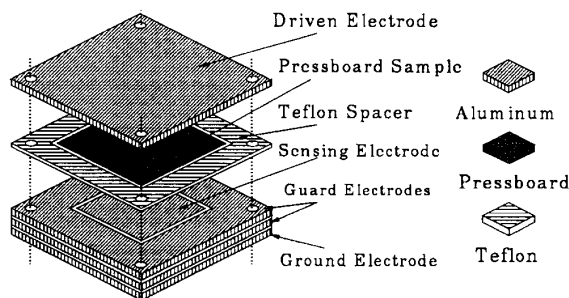

Figure 1.
Structure of the parallel-plate sensor.

fields, the guard electrodes serve to eliminate all parallel parasitic capacitances and resistances, which the sensing electrode might have with respect to the surrounding medium.

Another advantage to having a guard ring around the sensing electrode is that the electric field is highly uniform and there are essentially no fringing fields associated with that electrode. The material sample is larger in area than the sensing electrode, thus letting almost all field lines pass through the material sample. Teflon was chosen as the insulating material between the different electrodes because of its excellent thermal properties in addition to being a very good insulator. The entire 'sandwich' structure is tightened together with insulating nylon bolts.
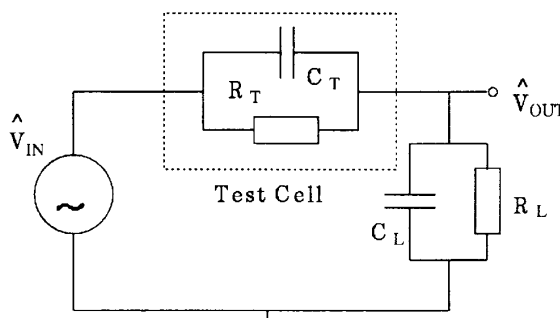

Figure 2.
Equivalent circuit of the test structure.

The input admittance, with which the sensing electrode is loaded, is that of a known parallel RC pair, modeled as shown in Figure 2 with

$$R_T = \frac{d}{\sigma A}$$
$$C_T = \frac{\epsilon A}{d} \tag{3}$$

where d is the plate separation distance, A is the sensing electrode area, and σ and ϵ are the material's conductivity and permittivity respectively.

For linear time-invariant (LTI) systems we take the standard complex frequency form

$$V_{IN} = \Re\{\widehat{V}_{IN}e^{i\omega t}\}$$
$$V_{OUT} = \Re\{\widehat{V}_{OUT}e^{i\omega t}\} \tag{4}$$

with complex amplitudes $\widehat{V}_{IN}$ and $\widehat{V}_{OUT}$ defined in Figure 2. A microprocessor-driven controller is responsible for generating the driving voltage and measuring the output voltage. The data that it produces are expressed in terms of a magnitude $20\log(M)$ [dB] and phase $\varphi \cdot 180/\pi$ [deg], which are related to the complex amplitudes defined in Figure 2 as

$$\frac{\widehat{V}_{OUT}}{\widehat{V}_{IN}} = Me^{i\varphi} \Rightarrow M = \left|\frac{\widehat{V}_{OUT}}{\widehat{V}_{IN}}\right|$$
$$\varphi = \angle\left(\frac{\widehat{V}_{OUT}}{\widehat{V}_{IN}}\right) = \arctan\frac{\Im\{\widehat{V}_{OUT}/\widehat{V}_{IN}\}}{\Re\{\widehat{V}_{OUT}/\widehat{V}_{IN}\}} \tag{5}$$

The next step in calculating σ and ε is to calculate R_T and C_T from measurements of M and φ, and the known values of R_L and C_L. We define the admittances of the test and load branches as $Y_T = 1/R_T + i\omega C_T$ and $Y_L = 1/R_L + i\omega C_L$ respectively. Then from the voltage divider relationship we obtain

$$\frac{\widehat{V}_{OUT}}{\widehat{V}_{IN}} = \frac{Y_T}{Y_T + Y_L}$$
$$= \frac{\frac{1}{R_T} + i\omega C_T}{\frac{1}{R_T} + \frac{1}{R_L} + i\omega(C_T + C_L)} = Me^{i\varphi} \tag{6}$$

In the low frequency limit as $\omega \to 0$, the voltage ratio becomes real and equal to $R_L/(R_L + R_T)$. In the high frequency limit as $\omega \to \infty$, the voltage ratio is also real and equal to $C_T/(C_T + C_L)$.

Solving (6) for R_T and C_T in terms of known values for R_L and C_L and measured values for M and φ yields

$$R_T = \frac{1 + M^2 - -2M\cos\varphi}{M[\cos\varphi - M - \omega R_L C_L \sin\varphi]}R_L \tag{7}$$

$$C_T = \frac{M[\cos\varphi - M + (1/\omega R_L C_L)\sin\varphi]}{1 + M^2 - 2M\cos\varphi}C_L \tag{8}$$

In order to test the performance of the parallel-plate sensor, we used it on known materials. For Shell Diala A transformer oil the results are shown in Figure 3. On a log-log scale, the plot of ε'' vs. frequency is a straight line of slope -1, which means that σ is independent of the frequency. This is characteristic of an ohmic material. For linear dielectric materials, ε' should also be constant with frequency. The observed rise of ε' at the lower end of the frequency range can be attributed to double layer formation at the aluminum-oil interface [4]. This plot
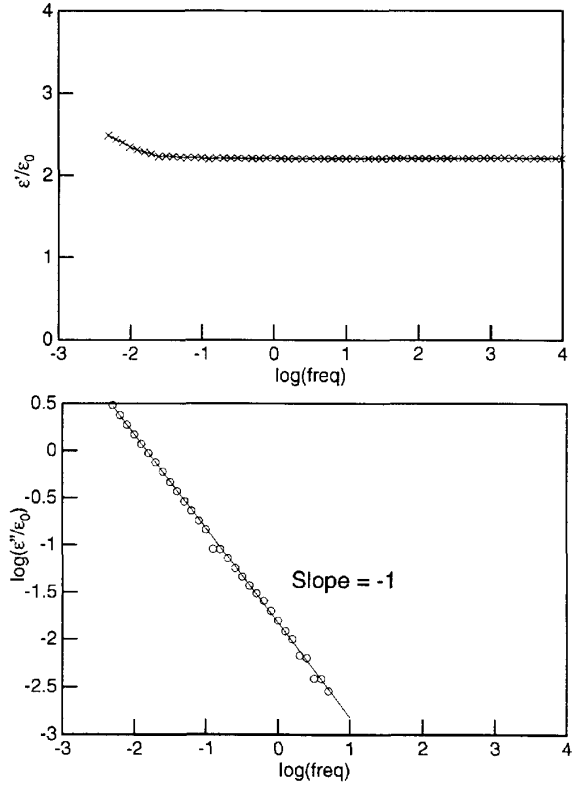

Figure 3.
Complex permittivity of transformer oil measured with the parallel-plate sensor.

corresponds to $\sigma = 0.83 \times 10^{-12}$ S/m and $\varepsilon/\varepsilon_0 = 2.2$, which are typical values for the dielectric parameters of transformer oil.

The plot of ε'' is not shown for frequencies higher than $10^{0.7}$ Hz. This is because at that frequency range the response is dominated by the capacitive element, and the gain/phase measurement is insensitive to the value of σ.

2.2. EXPERIMENTAL PROCEDURES

The objective of this set of experiments is to use the parallel-plate sensor to study how the dielectric spectrum of oil-impregnated pressboard changes with variations in temperature and moisture content. We first prepared many samples of pressboard, each with a different content of water. We then measured the moisture content of a small piece of each sample, placed the remaining sample in the sensor structure, scanned its dielectric spectrum at five different temperatures, and finally measured its moisture content again. This section describes all of these stages.

Prior to oil impregnation we cut 50×50 mm² pieces of 1 mm thick oil-free EHV-Weidmann HIVAL pressboard.

Then we placed them under vacuum, and subsequently in transformer oil, one at a time, for various lengths of time, in order to obtain different moisture contents. Table 2 lists the parameters of the oil-impregnation process that every sample underwent and the resultant moisture content.

The moisture of each sample was measured before and after the frequency scan using the Mitsubishi VA-05 water vaporizer and oven and the Mitsubishi CA-05 moisture meter. The small pressboard pieces cut from the samples were split into many thin layers before depositing in the vaporizer oven, which heated the pressboard samples to 180°C in order to drive out all of the moisture. This moisture was then entrapped in dry nitrogen gas and passed to the moisture meter for measurement. The optimal oven temperature of 180°C was chosen after a series of experiments to be a temperature where the moisture diffusion is fast enough so that the accuracy of the measurement is not compromised by the background titration rate of the moisture meter. At the same time the temperature is not so high, that the cellulose begins to disintegrate.

After the parallel-plate measurement, the entire remaining sample was used for the second moisture measurement. We define the moisture content of pressboard as the weight of water liberated from the sample during vaporization (a quantity provided by the moisture meter) divided by the total weight of the oil-impregnated sample before it is placed in the oven. If the two moisture measurements were not close to each other, the data of the sample was not used. This happened for samples NA, NC, and ME.

Measurements with every sample were taken at five temperatures: 30, 40, 50, 60, and 70°C. The parallel-plate sensor, with the pressboard sample placed inside it, is placed in an oven, whose temperature is controlled by a feedback temperature controller.

We have observed that in addition to a short (4 h) transient for the sample to reach thermal equilibrium, its complex permittivity experiences another, long transient. When we tested a sample for 270 h at a constant temperature (50°C) we observed the behavior illustrated in Figure 4. The long time constant of this transient suggested that it may be due to mass transfer processes of water in the pressboard. Since the sample in the test cell is sealed from the outside air, and since diffusion of water through 6 mm of pressboard before it reaches the active area would require months we concluded that this sample conditioning process is probably due to moisture redistribution within the bulk of the pressboard, finally resulting in a uniform distribution. Based on values for the diffusion constant taken from Table 1, namely
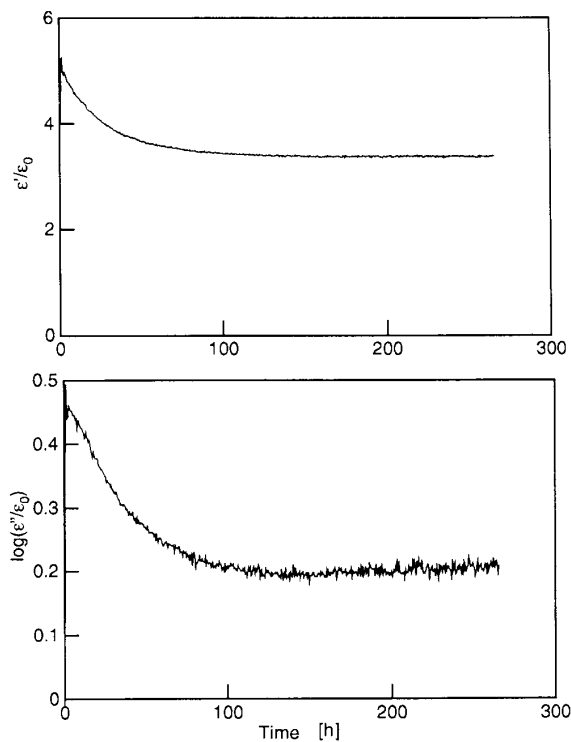

Figure 4.

Pressboard conditioning transient at 50°C and 0.860% moisture..

$D_p = 6.0 \times 10^{-12} \mathrm{m^2/s}$ at 70°C and $6.7 \times 10^{-14} \mathrm{m^2/s}$ at 15°C with $\Delta = 6$ mm. $\tau = \frac{\Delta^2}{D_p} = 69$ days to 17 years.

We then established the rule that after a sample is impregnated and placed in the test cell, it must stay there for at least five days at a temperature above 50°C before any measurements are performed.

2.3. RESULTS

We would like to establish a relationship between the temperature and moisture content of pressboard, and its dielectric spectrum. This can be accomplished by summarizing the results from frequency scans taken at several different moisture contents and temperatures.

Figure 5 shows the raw gain-phase data of a frequency scan of a representative oil-impregnated pressboard sample taken with the parallel-plate sensor. If we process the data shown in this Figure using (7) and (8) to produce values for the complex permittivity, we obtain the results shown in Figure 6.

The first thing to note in Figure 6 is that all ε'' data for frequencies $\gtrsim 10$ Hz is noise. This is due to the lack of sensitivity of the measurement at high frequencies to the

Table 2.

Impregnation process parameters for the pressboard samples used in the universal spectrum. Samples
NA, NC, and ME are not listed because the before and after moisture measurements greatly differed.

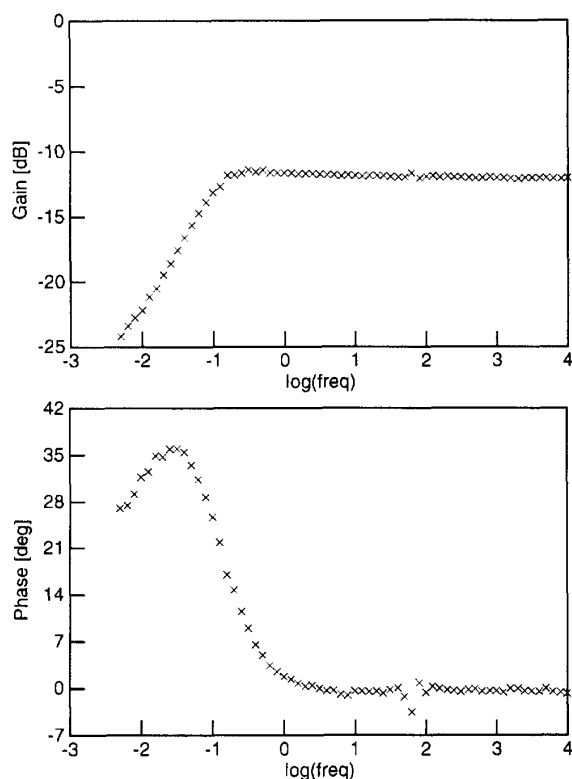| Sample | Vacuum Drying | | | Oil Immersion | | Moisture |
Name	T	Duration	Vacuum	T	Duration	
	[˚C]	[h]	[Pa]	[˚C]	[min]	[%]
NB	70	12		25	5×10^5	3.1
ND	70	24		70	60	1.1
MA	70	10	39.9	70	10	2.3
MB	70	2/3	53.2	60	10	1.8
MC	70	1/3	73.1	70	10	2.2
MD	70	2	26.6	70	10	0.42
MF	70	4	21.3	70	10	0.83
MG	70	15.5	13.3	70	10	1.8

Figure 5.

Raw gain-phase data for a frequency scan of a
representative pressboard sample MA at 50˚C
with $R_L = 9.78$ GΩ and $C_L = 123$ pF.

resistive component of the material. When we disregard
this data, the rest of the ϵ'' points lie approximately on
a straight line. This line does not have a slope of -1,
characteristic of an ohmic material. Instead, the slope is
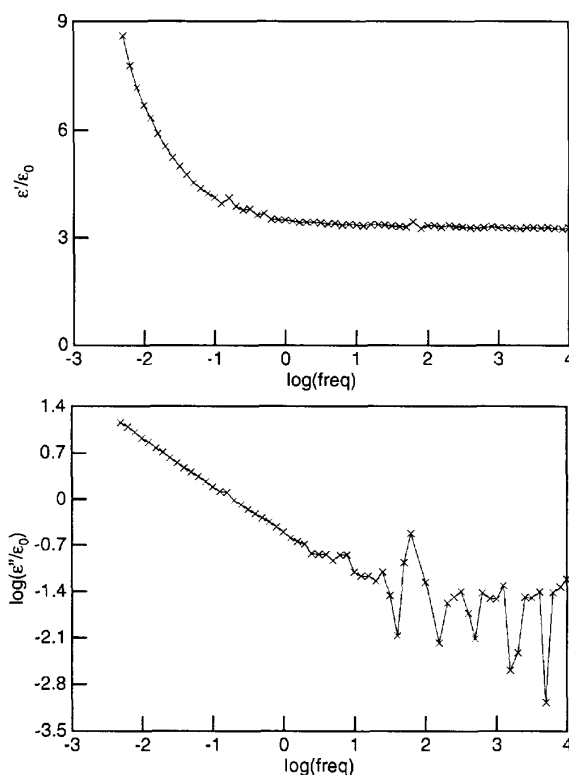≈ -0.7. This indicates that oil-impregnated pressboard
is dispersive.

Figure 6.

Dielectric spectrum of a representative press-
board sample MA at 50˚C.

This decay of ϵ'' is associated with a loss peak not
visible in Figure 6, because it occurs at a frequency be-
low the lower limit of our equipment (0.005 Hz). The
elevation in ϵ', which accompanies a loss peak in ϵ'', as
required by the Kramers-Kronig relations [8], is clearly
shown at the top of the Figure.

For seven samples the shape of the loss peaks in the

dielectric spectrum of a material is independent of moisture and temperature. The spectra only shift position with frequency. This allows the creation of a single 'universal' spectrum, to which all spectra map, after having been shifted (horizontally with frequency and/or vertically) by an amount which is a function of the temperature and moisture content [11, 12].

With only one loss peak, the entire spectrum could be described by the position of a single point, namely the peak itself, with coordinates $(\omega_p, \varepsilon_p^*)$. A shift in either ε' or ε'', both horizontally or vertically, is required by the Kramers-Kronig relations to be accompanied by an identical shift in the other component of ε^* [13, App. A]. It is unfortunate that the loss peak occurs at such low frequencies, because a degree of freedom is lost by having only a straight line to shift. In other words, ω_p and ε_p^* cannot be determined uniquely. We have therefore the freedom of choosing to shift the spectra either only horizontally, only vertically, or in some predetermined combination. We have chosen to move only horizontally, as suggested by previous research [12].

We chose a numerical method that fits the two spectra by trying shifts in increments of 0.1 on a logarithmic frequency scale, because this is the frequency resolution of our data acquisition system. It finds the shift that minimizes the sum of the squares of the differences between corresponding values of ε' and ε''.

First, let us look at the spectra of the same sample at different temperatures. Figure 7 is a plot of all five spectra of sample MA (Table 2). We have chosen sample MA at 50°C to be our reference spectrum. If we shift the other four spectra in Figure 7 by the appropriate amount, we obtain the universal curve at constant moisture for this sample shown in Figure 8.

One sample (NB), with the highest moisture content (3.1%), had spectra distinctly different from the rest, with a second loss peak visible, which implies either that over the extremely long process of impregnation of sample NB ($\sim$ 12 months) some kind of impurity has found its way into the pressboard, or that at higher moisture levels water exists in the pressboard in a different band state [13, 14]. Eliminating sample NB, we next collapsed the five spectra of every sample into universal curves of constant moisture. These universal spectra can now be shifted again to compensate for the moisture differences and to yield the final master universal spectrum shown in Figure 9, which contains data from 35 different frequency scans, seven samples of different moisture concentration at five temperatures each.

At the high-frequency end, the ε'' plots in Figure 9 show some spread, which is due to the high sensitivity to noise at these frequencies. Otherwise the thirty-five
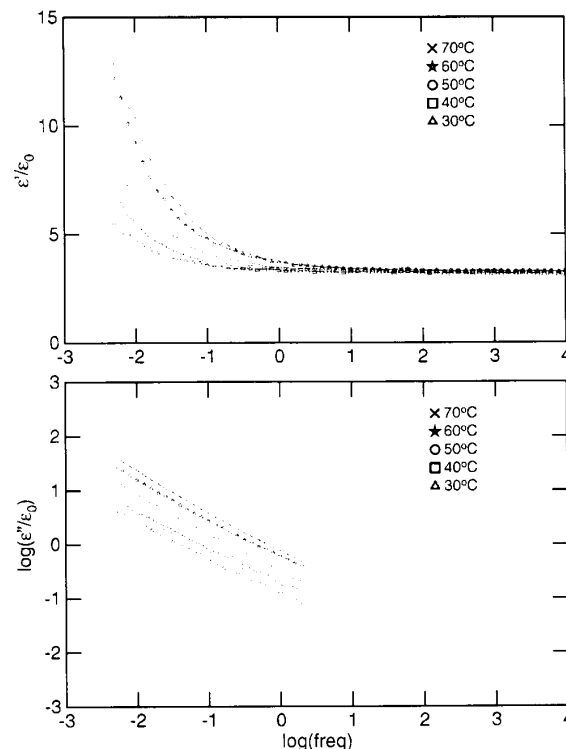

Figure 7.

Dielectric spectra of a pressboard sample (MA) at five temperatures with 23% moisture.

curves overlap quite closely. This universal mapping can be used to estimate the moisture content of pressboard, if its dielectric spectrum is measured at a known temperature. Table 3 lists the logarithmic frequency shifts by which each spectrum had to be shifted in order to form the master spectrum.

Table 3.

Relative logarithmic frequency shifts for data at different temperatures and moisture contents. Reference curves are at 50°C and 2.4% moisture (shown in bold).

Name	Moist	30°C	40°C	50°C	60°C	70°C
MD	0.42	−1.6	−1.3	−1.0	−0.7	−0.4
MF	0.83	−1.8	−1.3	−1.0	−0.7	−0.3
ND	1.1	−1.2	−0.9	−0.6	−0.3	0.1
MB	1.8	−1.3	−1.0	−0.6	−0.3	0.2
MG	1.8	−1.1	−0.7	−0.4	−0.2	0.1
MC	2.2	−1.4	−0.9	−0.5	−0.2	0.2
MA	2.4	−0.7	−0.4	0.0	0.4	0.5

In order to find out how the dielectric spectrum of pressboard changes with temperature and moisture content, we need to relate the logarithmic frequency shifts
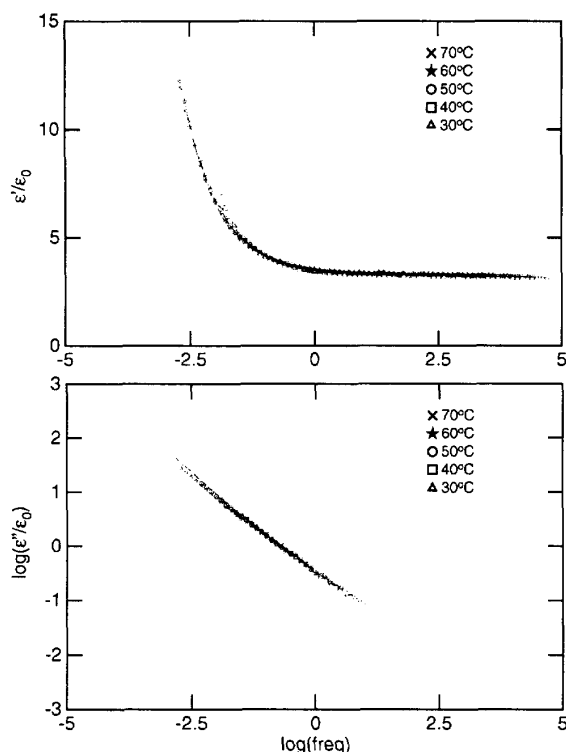
Figure 8.

Universal curve for one sample (MA) at five temperatures.

Figure 9.

Master universal spectrum, containing data from 35 frequency scans, shifted with moisture and temperature.

of Table 3 to the temperatures and moisture contents. In order to test whether the effects of either of these factors are independent of each other, we perform some processing on the data in Table 3. What the independence mentioned above implies is that one can assign a quantity of shift to every temperature and to every moisture, and the shift that every spectrum is subjected to is the sum of the shifts due to these two factors. Symbolically, this may be represented as follows

$$\log\left(\frac{\varepsilon' - \varepsilon_\infty}{\varepsilon_0}\right) = \mathcal{F}'\{\log\omega - [f_T(T) + f_M(m)]\} \quad (9)$$

$$\log\left(\frac{\varepsilon''}{\varepsilon_0}\right) = \mathcal{F}''\{\log\omega - [f_T(T) + f_M(m)]\} \quad (10)$$

where $f_T(T)$ depends only on the absolute temperature and $f_M(m)$ depends only on moisture. These formulas also incorporate the requirement that both components of ε^* shift by the same amount, as can be derived from the Kramers-Kronig Relations [13, App. A], [8].

The strategy applied to test the validity of the assumption that the shifts due to temperature and moisture are independent is to take every row in Table 3 and add to (or subtract from) every number in it the same amount in a way that would make the shift at 50°C be zero. This
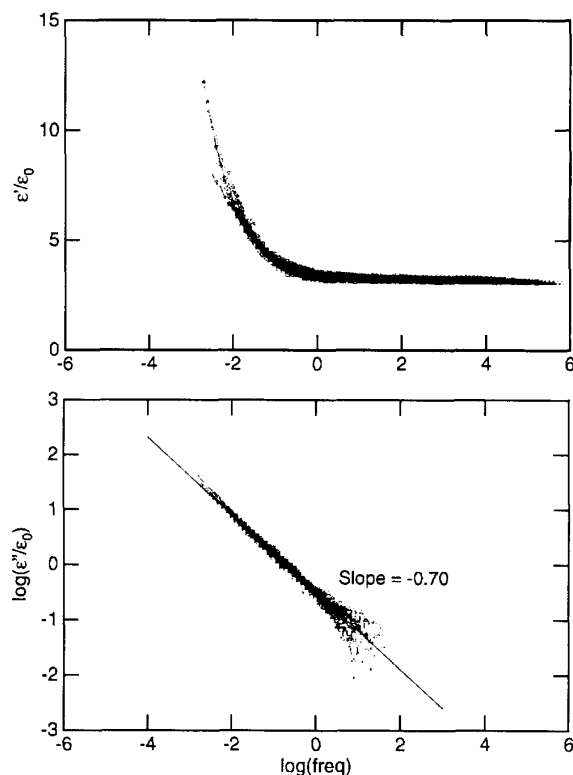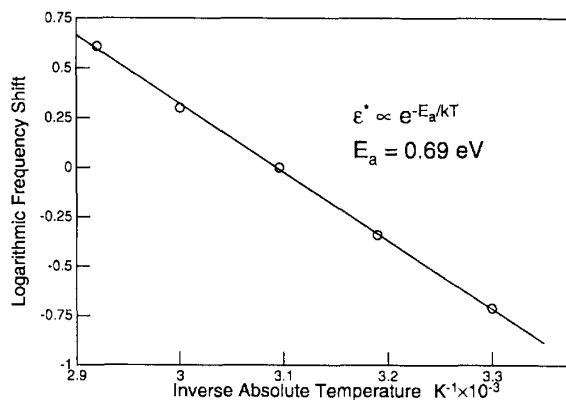

Figure 10.

Logarithmic frequency shift as a function of temperature: Arrhenius plot.

operation results in the numbers shown in Table 4. We have normalized the data in such a way that the effect of moisture has been eliminated. If the two effects are truly independent of each other, the numbers in each column of

Table 4 would be approximately the same, which would represent the frequency shift due to temperature alone. We can see in Table 4 that this is approximately true. We can now take the average of the numbers in each column to be the logarithmic shift due to temperature, as plotted in Figure 10.

Table 4.

In this table the spectra for all moisture contents have been shifted so that all of the 50°C curves overlap. In this way the effects due to moisture have been eliminated and one can calculate the average shift due to temperature.

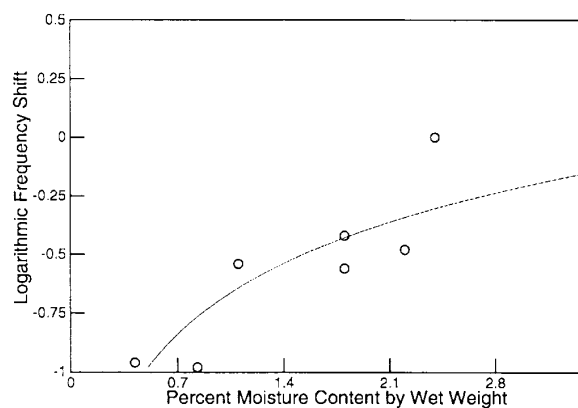| %	30°C	40°C	50°C	60°C	70°C
0.42	−0.6	−0.3	0.0	0.3	0.6
0.83	−0.8	−0.3	0.0	0.3	0.7
1.1	−0.6	−0.3	0.0	0.3	0.5
1.8	−0.7	−0.4	0.0	0.3	0.8
1.8	−0.7	−0.3	0.0	0.2	0.5
2.2	−0.9	−0.4	0.0	0.3	0.7
2.4	−0.7	−0.4	0.0	0.4	0.5
Average	−0.71	−0.34	0.0	0.30	0.61

Figure 11.

Logarithmic frequency shift as a function of moisture. The curve represents a best fit to this data according to the chosen functional form (26) in Section 4.4.2.

We can similarly eliminate the effects of temperature by making the entire row in Table 3 for MA be all zeros, by adding or subtracting the appropriate amount from each number in the same column. The results of this operation are shown in Table 5. From this table we can now calculate the average logarithmic shift due to moisture, as plotted in Figure 11. In conclusion we can say that the two factors independently shift the dielectric spectrum of pressboard.

One can see in Figure 10 that the relationship between inverse temperature and logarithmic frequency shift is

Table 5.

The spectra for all temperatures have been shifted so that all of the 2.4% (MA) curves overlap. In this way the effects due to temperature have been eliminated and one can calculate the average shift due to different moisture contents.

%	30°C	40°C	50°C	60°C	70°C	Ave.
0.42	−0.9	−0.9	−1.0	−1.1	−0.9	−0.96
0.83	−1.1	−0.9	−1.0	−1.1	−0.8	−0.98
1.1	−0.5	−0.5	−0.6	−0.7	−0.4	−0.54
1.8	−0.6	−0.6	−0.6	−0.7	−0.3	−0.56
1.8	−0.4	−0.3	−0.4	−0.6	−0.4	−0.42
2.2	−0.7	−0.3	−0.5	−0.6	−0.3	−0.48
2.4	0.0	0.0	0.0	0.0	0.0	0.0

approximately linear over the small measured temperature range. If we assume the Arrhenius dependence $\epsilon^* \propto e^{-E_a/kT}$, where k is Boltzmann's constant, then the plot of Figure 10 corresponds to an activation energy of $E_a \approx 0.69$ eV.

2.4. ALGORITHM FOR USING THE UNIVERSAL SPECTRUM

Suppose that we perform a dielectrometry measurement on a sample of pressboard at a known temperature. How can we use the results presented in Section 2.3 to find its moisture content?

We first need to determine what positive or negative frequency shift would map this spectrum onto the reference spectrum MA at 50°C. If the dielectrometry is performed only at a single frequency, then Figure 9 can be used to determine at what frequency the corresponding value of ϵ^* is achieved, and the frequency shift will be equal to the difference between these two frequencies.

The next step is to find the frequency shift associated with the temperature of the sample. This may be done graphically in Figure 10. The shift due to temperature is then subtracted from the total shift and the result is the shift due to moisture. Finally, the right most column of Table 5 is used to estimate what moisture content would correspond to this frequency shift.

3. THE FLEXIBLE THREE-WAVELENGTH INTERDIGITATED SENSOR

The flexible three-wavelength sensor has been used in past preliminary studies to measure one-dimensional spatial variations in the complex permittivity [4]. We report on our efforts to improve further this technique.
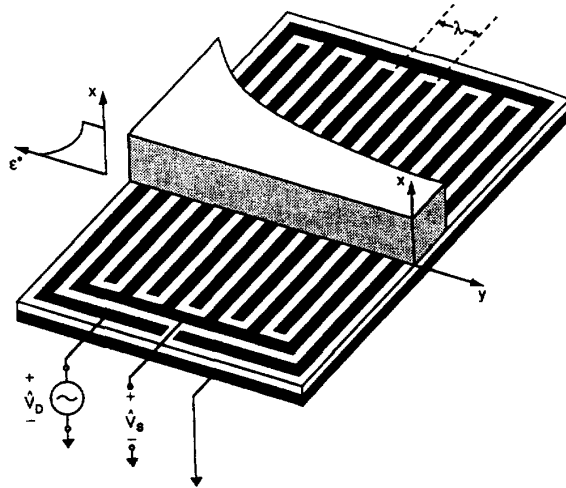
Figure 12.   Imposed ω-k dielectrometry [4].

3.1. IMPOSED ω-k DIELECTROMETRY

If electrodes are placed side by side in a repeating pattern on one surface of the material, the electric fields will decrease away from the electrodes and the complex impedance between the electrodes will be most sensitive to the material adjacent to them.

In previous work [1, 2, 4] periodic electrode structures with a multitude of interdigitated fingers, as shown in Figure 12 have been designed. The electric fields are uniform in the z direction and periodic in the y direction with a spatial wavelength of λ, equal to the distance between repeating electrodes. Thus at every surface of constant x the electric potential is periodic in y and can be expanded as an infinite series of sinusoidal Fourier modes of spatial wavelengths $\lambda_n = \lambda/n$. This is very convenient, because the two-dimensional solutions to Laplace's equation

$$\nabla^2 \Phi = 0 \tag{11}$$

in Cartesian geometry are of the form

$$\Phi = \sum_{n=1}^{\infty} \Phi_n \operatorname{hyp}(k_n x)\operatorname{trig}(k_n y) \tag{12}$$

where $k_n = 2\pi/\lambda_n$ is the wavenumber of the nth mode, $\operatorname{hyp}(x)$ stands for any one of the hyperbolic exponential functions $\sinh(x)$, $\cosh(x)$, e^x, or e^{-x}, and $\operatorname{trig}(y)$ stands for one of the trigonometric functions $\sin(y)$ or $\cos(y)$. For every Fourier mode n, the electric fields decrease with x as $\exp(-2\pi n x/\lambda)$ with the fundamental mode $n = 1$ penetrating farthest into the material.

By designing sensors with various fundamental spatial wavelengths λ, it is possible to test the dielectric properties of materials at different depths. Combining the

results from several such sensors makes it possible to determine the x dependent spatial profiles of the complex permittivity.
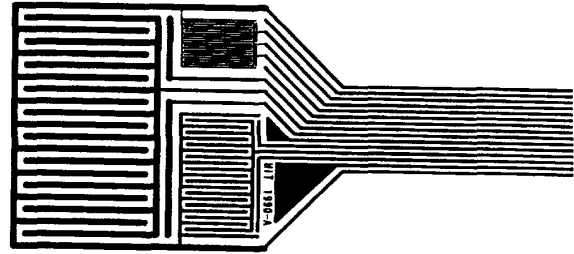

Figure 13.

Structure of the three-wavelength interdigitated sensor as designed by von Guggenberg [4].

3.2. SENSOR STRUCTURE AND PRELIMINARY MEASUREMENTS

The flexible three-wavelength sensor structure is shown in Figure 13. It consists of three sets of interdigitated electrodes, deposited on a common flexible Kapton™ (a polyimide) substrate. Every set of electrodes contains ten wavelengths. The area of the active surface is $\sim 5 \times 5$ cm². In a way similar to the parallel-plate sensor (Section 2.1), the sensing electrodes of every wavelength are shielded by guard electrodes, driven by a buffer stage, and the guard electrodes are shielded by ground electrodes.

On the bottom surface of the substrate a copper ground plane is deposited, which is electrically connected to the ground electrodes. The entire sensor is coated with Parylene™, a hydrophobic polymer, which serves to protect the sensor from contamination. Table 6 lists the physical parameters of the three-wavelength sensor and the load impedances [4, Sect. 6.3].

Table 6.

Nominal values of parameters describing the three-wavelength sensor and load impedances [4].

Parameter	Values		
Spatial wavelength λ	1.0 mm	2.5 mm	5.0 mm
Interelectrode spacing	0.24 λ	0.24 λ	0.24 λ
Electr. meander length	0.15 m	0.15 m	0.30 m
Substrate thickness	127 μm	127 μm	127 μm
Substrate permitt. ε_s	3.0 ε_0	3.0 ε_0	3.0 ε_0
Parylene layer thickness	5.0 μm	5.0 μm	5.0 μm
Permitt. of Parylene ε_p	3.05 ε_0	3.05 ε_0	3.05 ε_0
Load Capacitance C_L	226 pF	37.6 pF	6.47 pF
Load Resistance R_L	∞	∞	∞

A mathematical model relates the gain/phase response of an interdigitated sensor to its physical parameters, the

medium above it, and the frequency of excitation. This two-dimensional problem is solved with the help of numerical techniques. Details of this process are presented in [1] and [2].
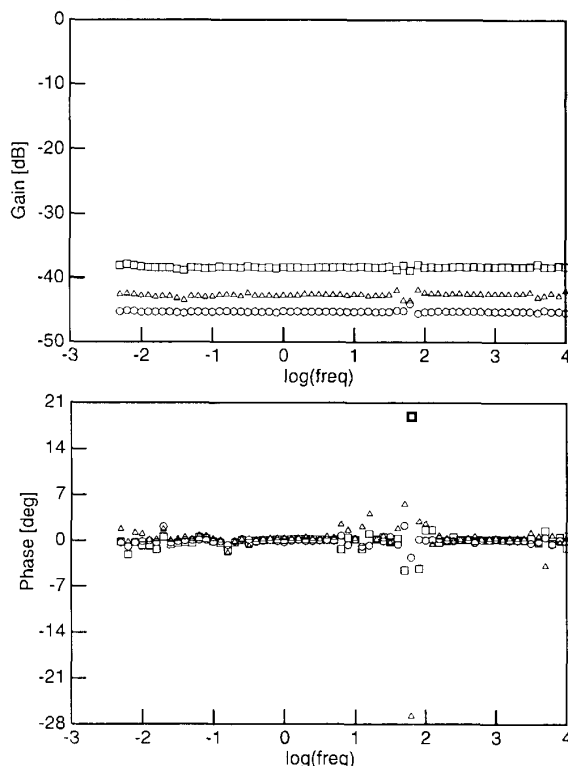

Figure 14.

Response of a three-wavelength sensor in air before Parylene coating and after recommended chemical cleaning procedure and heating. It shows zero phase and constant gain over the entire frequency range, indicating a clean sensor. $\triangle$ $\lambda = 5$, $\square$ $\lambda = 2.5$, $\bigcirc$ $\lambda = 1$ mm.

Figure 14 shows measurements in air that verify that the sensor has no surface contamination, with a zero phase angle and constant gain for each wavelength over the measured frequency range. Figure 15 shows representative three wavelength gain/phase data in transformer oil and Figure 16 shows the corresponding values of ε' and ε''. For these measurements we have $\varepsilon/\varepsilon_0 = 2.2$ and $\sigma \approx 1.4 \times 10^{-12}$ S/m. In a uniform medium each of the three wavelength measurements should give the same values of ε' and ε''.

4. PARAMETER ESTIMATION ALGORITHMS

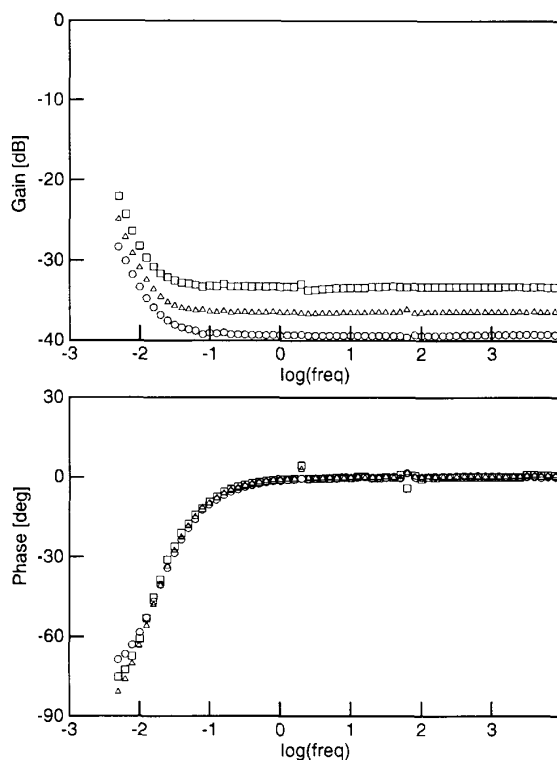Numerical techniques can be used to solve the forward problem of calculating the magnitude and the phase an-

Figure 15.

Raw gain-phase data of the three-wavelength sensor in Shell Diala A transformer oil. $\triangle$ $\lambda = 5$, $\square$ $\lambda = 2.5$, $\bigcirc$ $\lambda = 1$ mm.

gle of the voltage ratio of an interdigitated sensor from the parameters of the sensor and the properties of the materials above it. What is meant by parameter estimation is the reverse problem of finding properties of the materials from measured magnitude and phase data. Numerical techniques must be used for this purpose, since it is impossible to express this solution in closed form. In this Section we review the various techniques for parameter estimation that have been developed and tested.

In Section 4.1 we discuss how some qualitative information about the spatial variations of the dielectric properties of a material can be obtained from the comparison of data taken with interdigitated sensors of several different spatial wavelengths. The next step would be to try to combine the results from all of these wavelengths in a quantitative manner, in order to calculate this spatial variation.

The first question is how much information can be obtained from measurements with the same wavelength at different frequencies. Reference [1, pp. 88] summarizes in
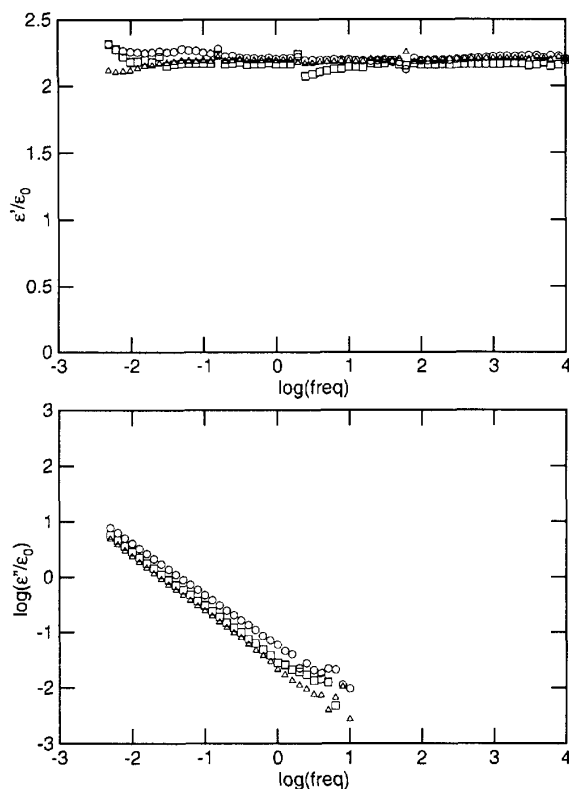
Figure 16.

Dielectric spectrum of Shell Diala A transformer oil taken with the three-wavelength sensor shows that the oil is spatially uniform as each wavelength has essentially the same value of permittivity $\epsilon \approx 2.2\epsilon_0$ and conductivity $\sigma \approx 1.4 \times 10^{-12}$ S/m. The results include all significant spatial Fourier modes. $\triangle \lambda = 5$, $\square \lambda = 2.5$, $\bigcirc \lambda = 1$ mm.

Theorem 3.2 that a unique determination of the complex permittivities in a structure consisting of several homogeneous layers is possible only if the relaxation times of the materials are sufficiently distinct and they appear in decreasing order as one moves away from the electrode surface. This constraint makes this approach useful only in specific cases, where the material layers are in the required order.

Given that this is the case, we next investigate how measurements with sensors of different spatial wavelength at the same frequency can be combined to calculate some unknown parameters of the medium above the sensors. Different ways to accomplish this are presented in Sections 4.2, 4.3, and 4.4.

4.1. ONE-DIMENSIONAL PARAMETER ESTIMATION

This is the simplest kind of parameter estimation in which only one complex parameter is unknown, namely the complex permittivity ϵ^* of one of the layers above the interdigitated sensor. The algorithm takes data from one wavelength and uses a root-finding algorithm to find the unknown parameter [1]. The gain and phase of the response are a function of the unknown ϵ^*. The problem is that of finding a root (zero) of the difference of this function and the measured results.

An arbitrary number of known layers may be included along with the unknown layer, i.e. no unnecessary assumptions need to be made about the structure of layers, other than the assumption that the unknown layer's dielectric properties do not change with variations in x.

If the material is indeed homogeneous, then sensors of any spatial wavelength would measure the same value of ϵ^*. If, however, ϵ^* depends on x, then the value of ϵ^* measured by an interdigitated sensor would be some sort of a weighted average, with the depth of sampling proportional to the spatial wavelength λ of the sensor. Consequently, if a material is not homogeneous, each different wavelength electrode structure of the three-wavelength sensor would measure different values of ϵ^*.

Although this method can show homogeneity if all three wavelengths give the same ϵ^*, if the material is inhomogeneous it can only provide a qualitative picture of how ϵ^* varies with x. It is nevertheless a very useful tool and is probably the first step to take when interpreting dielectric profile data. Section 5 shows instances of the application of this method to data from measurements.

4.2. MARCHING APPROACH

This is the first method which attempts to combine the results from more than one wavelength into a quantitative description of the spatial dielectric profile of an inhomogeneous medium. It is presented in detail in [15]. Its iterative algorithm is based on a series of one-dimensional estimations of the kind described in Section 4.1 and thus avoids the complications associated with multidimensional searches.

This method approximates the dielectric profile of the structure above it by a stair-step function, with the intervals of this function being determined by the algorithm itself. It is therefore only applicable to the problem of finding an approximation to the dielectric profile of one single unknown layer extending to infinity, as no a priori information may be specified about the widths of the different regions.

An assumption is made that every sensor of spatial wavelength λ has a depth of penetration into the material equal to $\alpha\lambda$, where α is a parameter which reflects the assumed discreteness of the regions. Each subsequent sensor in order of increasing wavelength is therefore assumed to be sensitive to one more layer than the previous one and this reduces the problem to that of many one-dimensional searches. The algorithm makes several runs through all distinct wavelengths until convergence, if possible, is reached.

The greatest advantage of this method lies in its relative simplicity in that it avoids multidimensional searches by only solving for one unknown at a time. This also makes it somewhat more robust in terms of convergence than the multidimensional searches. However, this method does not allow for the specification of structures with layers of arbitrary thickness or the inclusion of known layers. The marching approach is perfectly fitted to situations where a single inhomogeneous material is in intimate contact with the interdigitated electrodes and its thickness is greater than the reach of the longest wavelength.

4.3. MULTI-DIMENSIONAL PARAMETER ESTIMATION

This is a process which searches for more than one unknown variable simultaneously. It is useful in cases when there are more than one unknown layer in a material structure and data from more than one spatial wavelength is available. There are no limitations to the thicknesses or the position and order of the unknown layers.

An inhomogeneous layer may be approximated by a number of unknown homogeneous layers forming a stair-step function in a way similar to the marching approach of Section 4.2. However, in this case these sublayers may be assigned arbitrary thicknesses in a way that would approximate the profile function more closely.

4.3.1. A ROOT-FINDING ALGORITHM

In this method we are looking for exact solutions for the complex permittivity of the unknown layers. Two degrees of freedom are necessary for every unknown layer (ε, σ) and two degrees of freedom are assigned to every spatial wavelength (M, φ), which means that the number of unknown layers must be equal to the number of spatial wavelengths. The three-wavelength sensor can therefore be used to measure the complex permittivities of three unknown homogeneous layers above it.

Every measurement with a specific spatial wavelength λ_i creates one complex equation of the form

$$f_i(\varepsilon_1^*, \varepsilon_2^*, \dots) = \widehat{M}_i^c(\varepsilon_1^*, \varepsilon_2^*, \dots) - \widehat{M}_i^m = 0 \qquad (13)$$

where the functions $\widehat{M}_i^c$ represent the forward process of evaluating the complex gain from the layer structure and $\widehat{M}_i^m$ is the measured value of the complex gain. This is how one equation in the set of equations results from every spatial wavelength.

The root-finding algorithm is based on a hybrid between the Newton-Raphson and the Secant methods [16]. The Jacobian matrix and its inverse are not calculated for every iteration, but the old matrix is used for several iterations before a new one is computed.

Since the Newton-Raphson and the Secant methods may become unstable and severely deviate from a root, it is necessary to introduce damping to the algorithm. After a new guess is computed, a test is performed to determine whether the new guess is closer to the root than the old one. A vector X is considered closer to the root of the system of equations if the absolute value of its corresponding result vector Y is smaller. If the new guess is not closer, then a half step backward is taken. If this guess is still worse than the old one, a quarter step back is taken, *etc.* If more than five such steps are needed, we conclude that a new Jacobian matrix needs to be calculated. Also, if this matrix is already up to date, but still damping does not get a better guess, the method fails and no solution is found.

Since in the process of finding new values for the unknown parameters the inverse of the Jacobian matrix is calculated, this matrix must be non-singular, which is similar to the requirement that the slope be non-zero in the one-dimensional Newton-Raphson method. This means that at least one unknown layer must fall within the reach of every sensor and every unknown layer must fall within the reach of at least one sensor. Although this is a necessary requirement to find a solution, it might not be a sufficient condition for a non-singular matrix. We have not, however, been able to find a situation when the method would fail due to such a problem.

The iterations stop either when the absolute value of the result vector is less than a prespecified tolerance, or when the new iteration yields a new guess which is very close to the old one.

Convergence case studies of this method indicated that convergence is always reached if every unknown layer is well within the scope of at least one sensor. We applied this method to computer-generated complex gain data, which simulated two layers with various values of the conductivity and the permittivity and with various initial guesses for layer 1. Convergence was reached in all cases. Table 7 lists the parameters of these tests, as well as the total number of iterations # that were necessary to find the root. We also tested the behavior of

Table 7.

Computation time of the root-finding algorithm as a function of initial guess and solution using multidimensional estimation. The frequency is 0.01 Hz. Negative values for final result conductivity are small variations about zero due to 'numerical' noise.

Try	Layer	Initial guess ε	σ	True values ε	σ	Final result ε	σ	#	Time [m:s]
1	1	8.85×10^{-12}	0	8.85×10^{-12}	0	8.84×10^{-12}	-9.91×10^{-15}	5	1:49
	2	8.85×10^{-12}	0	8.85×10^{-12}	10^{-12}	8.86×10^{-12}	1.00×10^{-12}		
2	1	8.85×10^{-12}	0	8.85×10^{-12}	0	8.85×10^{-12}	4.57×10^{-15}	9	4:21
	2	8.85×10^{-12}	10^{-11}	8.85×10^{-12}	10^{-12}	8.85×10^{-12}	1.00×10^{-12}		
3	1	8.85×10^{-12}	0	8.85×10^{-12}	0	8.85×10^{-12}	-3.96×10^{-15}	7	3:08
	2	5×10^{-11}	0	8.85×10^{-12}	10^{-12}	8.86×10^{-12}	1.00×10^{-12}		
4	1	8.85×10^{-12}	0	8.85×10^{-12}	0	8.83×10^{-12}	0	5	1:56
	2	8.85×10^{-12}	0	3×10^{-11}	0	3.00×10^{-11}	0		
5	1	8.85×10^{-12}	0	8.85×10^{-12}	0	8.85×10^{-12}	1.67×10^{-17}	9	4:12
	2	8.85×10^{-12}	10^{-11}	3×10^{-11}	0	3.00×10^{-11}	-2.28×10^{-17}		
6	1	8.85×10^{-12}	0	8.85×10^{-12}	0	8.77×10^{-12}	0	7	3:28
	2	5×10^{-11}	0	3×10^{-11}	0	3.00×10^{-11}	0		

this estimation process if an intentional error was introduced to the computer-generated data. The results of these tests are shown in Table 8. Noise at the input naturally resulted in noise in the output, but did not seem to affect the ability of the algorithm to find ε^* solutions. It is conceivable that instrumentation errors inherent in every measurement might cause the problem to have no solution. This obstacle could then be overcome by allowing for a larger tolerance in the convergence test. The negative values for the conductivity in Tables 7 and 8 are small variations about zero due to 'numerical' noise.

As mentioned earlier, a new Jacobian matrix is calculated every several iterations. The root-finding method is closer to the Newton-Raphson method if a new Jacobian is computed more often, while if J is rarely updated the method is closer to the Secant method. The former converges much faster, but the calculation of the Jacobian costs a lot of extra computation time. These are two competing factors in terms of computation time cost. Tests have shown [13] that for this set of data convergence is reached fastest if a new Jacobian was calculated at every step, in spite of all the extra computation associated with this. However, if there is a large number of unknowns this may no longer be true, since the number of computations associated with finding the Jacobian increases with the square of the number of unknowns.

4.3.2. AN OPTIMIZATION ALGORITHM

If we have more sensors than unknown layers the problem becomes overspecified, *i.e.* the set of equations will in general have no solution. However, the extra information should in principle contribute to finding an even closer approximation to the profile function. Therefore the problem is one of optimization, *i.e.* finding the set of values for all of the unknown complex permittivities that would minimize the set of functions f_i defined in (13). The function that we are trying to minimize is given as the sum of the squares of all of the individual functions

$$F = \sum_{i=1}^{N} |f_i(\varepsilon_1^*, \varepsilon_2^*, \ldots)|^2$$

$$= \sum_{i=1}^{N} |\widehat{M}_i^c(\varepsilon_1^*, \varepsilon_2^*, \ldots) - \widehat{M}_i^m|^2 \qquad (14)$$

In theory, if the data is error-free, such as computer-generated data, then the problem would have a solution even if it is overspecified, because the extra measurements would be redundant. However, unlike the case of equal number of degrees of freedom, adding experimental noise to an overspecified problem will lead to no solution. This is when the optimization method becomes extremely useful. Adding more wavelengths would act to reduce the effects of measurement noise.

Optimization techniques have the additional advantage that they tend to be much more stable than root-finding methods. They do have one major drawback. Although there may be many local minima, and so one can never be sure that the global minimum has been found. It is therefore of a crucial importance to begin with a guess very close to the true solution.

Case studies [13] showed that our implementation of an optimization algorithm, based on the Simplex Method [16] takes longer to arrive at the solution than the root-finding method, and that the optimization algorithm can

Table 8.

Effect of noise on the results from the multidimensional parameter estimation for two sensors $\lambda = 2.5$ mm (index 1) and $\lambda = 1.0$ mm (index 2), and two layers: top, $d = \infty$ (index 1) and bottom, $d = 0.25$ mm (index 2). The input values in bold are the ones that have been altered. The exact values are given in the top entry labelled 'No noise'. The frequency is 0.01 Hz. Negative values for final result conductivity are small variations about zero due to 'numerical' noise.

Index		Input		Output	
	$\downarrow$	g [dB]	ϕ [°]	ε	σ
No	1	−38.30	−43.68	8.85×10^{-12}	0.0
noise	2	−41.40	−57.98	8.85×10^{-12}	1.0×10^{-12}
	1	−38.30	**−45**	8.72×10^{-12}	1.03×10^{-14}
	2	−41.40	−57.98	8.88×10^{-12}	9.98×10^{-13}
	1	−38.30	−43.68	7.63×10^{-12}	-9.64×10^{-14}
	2	**−40**	−57.98	1.09×10^{-11}	1.17×10^{-12}
	1	−38.30	−43.68	9.10×10^{-12}	-2.66×10^{-14}
	2	−41.40	**−60**	8.31×10^{-12}	1.02×10^{-12}

give wrong answers, because it arrives at different local minima than the one corresponding to the true solution.

4.4. ASSUMED PROFILE FUNCTION ESTIMATION

So far we have approximated a dielectric profile by stair-step functions. This is the simplest and a very general kind of approximation. It makes it possible to use the existing models, which assume that the medium above the interdigitated electrodes consists of a set of homogeneous layers to approximate an inhomogeneous layer.

These methods provide no means of using a priori knowledge about the functional form of the dielectric profile in the parameter estimation. If we know that a function has a specific form, then we may be able to find this function exactly with only a limited number of degrees of freedom. If we know nothing about a function, then we would need an infinite number of degrees of freedom to determine it exactly, because only an infinite set of equations would let us decrease the width of the intervals in the stair-step function to zero.

In this Section we investigate the functional form of dielectric profiles in pressboard, which result from moisture mass transfer processes. We already know from Section 2 how the complex permittivity of pressboard depends on its moisture content. What remains to be seen is what profiles the moisture content in pressboard may assume.

4.4.1. DIFFUSION EQUATION

We are only considering diffusion in one dimension. This is justified by the fact that we are interested in modeling processes that occur in high-power transformers, where the pressboard appears in thin sheets, with one surface in contact with the oil. The thickness of these sheets is very small compared to their other dimensions
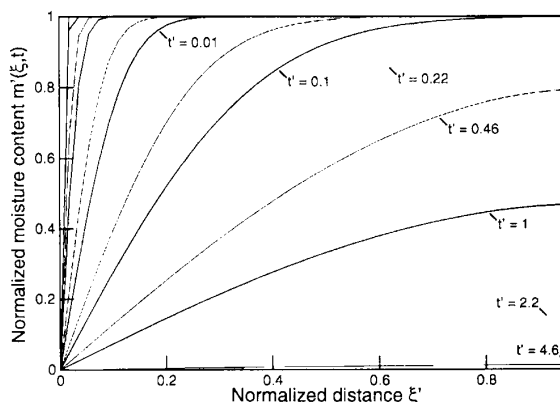

Figure 17.

Solutions to the diffusion equation for normalized moisture content $m'(\xi, t) = m(\xi, t)/m_0$ with $m_1 = 0$ at different values of normalized time $t' = (\pi^2 Dt)/(4d^2)$ as a function of normalized distance $\xi' = \xi/d$.

and therefore we assume that the moisture content depends only on the transverse coordinate ξ. In this case the diffusion of water in pressboard is governed by

$$\frac{\partial m}{\partial t} = \frac{\partial}{\partial \xi}\left[D(m)\frac{\partial m}{\partial \xi}\right] \qquad (15)$$

where m is the moisture concentration and $D(m)$ is the diffusion coefficient, which is, in general, a function of the moisture. This fact introduces a nonlinearity in (15) which would make it very difficult to solve. Since our goal is to obtain only the general form of the functional dependence, we shall assume from now on that $D(m)$ is a constant. Since there may be other layers, such as the Parylene coating, between the pressboard sheet and the electrodes, it is convenient to define ξ such that $\xi = 0$
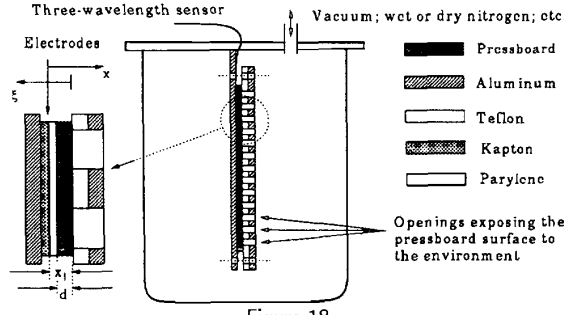
Figure 18.

Experimental setup for profile measurements taken with the 3-λ sensor.

at the exposed outer surface of the pressboard, and $\xi = d$ at the sealed surface, where d is the thickness of the pressboard sample. If the distance between the exposed surface and the sensor is x_1, then $\xi = x_1 - x$ (Figure 18).

The closed-form solutions to (15) are

$$m(\xi, t) = \begin{cases} e^{-Dk^2t} \sin k\xi \\ e^{-Dk^2t} \cos k\xi \\ \text{erf}\left(\frac{L-\xi}{2\sqrt{Dt}}\right) \\ \text{erf}\left(\frac{L+\xi}{2\sqrt{Dt}}\right) \end{cases} \quad (16)$$

where k is the diffusion equation separation constant and L is an arbitrary parameter. These solutions are pairwise independent, *i.e.* either pair of equations may be used to find the total solution of a diffusion problem. The error function erf(x) is defined as [17]

$$\text{erf}(x) = \frac{2}{\sqrt{\pi}} \int_0^x e^{-\eta^2} d\eta \quad (17)$$

and it has the bell curve as its derivative. In most cases infinite sums of these functions are needed to match boundary conditions and particular solutions. The first two forms are more convenient at times longer than the characteristic diffusion time $\tau = d^2/D$, where d is the thickness of the layer, while the last two forms are more convenient at times shorter than τ, when a change at one surface has not had the time to significantly diffuse to the other.

Let us assume that the exposed surface at $\xi = 0$, *i.e.* the surface of the pressboard in contact with the oil, is constrained by the equilibrium with oil (Section 1.3) to be at a certain constant concentration, and that this concentration experiences a step change at time $t = 0$ from m_0 to m_1 such that

$$m(\xi = 0, t < 0) = m_0 \quad (18)$$

$$m(\xi = 0, t > 0) = m_1 \quad (19)$$

We are also assuming that all previous transients in the moisture distribution have had time to die away such that at $t = 0^-$ the moisture is uniformly distributed, *i.e.*

$$m(\xi, t = 0^-) = m_0 \quad (20)$$

At the other surface, $\xi = d$, there is no moisture flux, since it is sealed by the sensor, so that

$$\frac{\partial m}{\partial \xi}(\xi = d, t) = 0 \quad (21)$$

We recognize that out of the solutions to the diffusion equation, only the top solution in (16) satisfies these boundary conditions, for values of $k_n = (n\pi)/(2d)$, with n a positive odd integer. A sum of terms with the above values for k constitute the homogeneous part of the solution to this differential equation. The particular solution is $m_p(\xi, t) = m_1$. Since at time $t = 0$ the moisture distribution is given by (20) except at $\xi = 0$, where $m(\xi = 0, t = 0) = m_1$, we must find an infinite series with terms in the top form of (16), which would converge to this function. We therefore use a Fourier sine series expansion to write the total solution to the differential equation:

$$m(\xi, t) = m_1 + (m_0 - m_1) \sum_{n=1,\text{odd}}^{\infty} \frac{4}{\pi n} e^{-Dk_n^2 t} \sin k_n \xi \quad (22)$$

Figure 17 shows a family of functions in the form of (22), every curve corresponding to a specific value of normalized time $t' = (\pi^2 Dt)/(4d^2)$. As is clear from (22), higher order modes die out with time at a considerably higher rate as compared to lower modes due to the factor k_n^2 in the exponential. At large values of the normalized time one can see that only the fundamental spatial mode of the transient is present, which is simply a one-quarter period of a sine in space.

Based on (22) we may assume that the general moisture concentration in the pressboard sample at some instant of time is of the functional form

$$m(\xi) = A + B \sum_{n=1,\text{odd}}^{\infty} \frac{4}{\pi n} e^{-Dtk_n^2} \sin k_n \xi \quad (23)$$

4.4.2. PROFILE FUNCTIONS

Equations (9) and (10) show how the dielectric spectrum of pressboard varies with changes in its moisture content. For the moisture contents of interest, *i.e.* for contents $\lesssim 3\%$, the loss peak in pressboard occurs at frequencies below 0.005 Hz (Section 2.3), and the only part of the dielectric spectrum visible is the decrease to the

right of the loss peak, which on a log-log plot is a straight line of slope $\gamma \approx -0.7$ (Figure 9). We may therefore write

$$\mathcal{F}'(\eta) = c_1 + \gamma\eta \qquad (24)$$

$$\mathcal{F}''(\eta) = c_2 + \gamma\eta \qquad (25)$$

where c_1, c_2, and γ are constants. Before we are ready to write the general equation relating ε^* to the moisture content m, we need to know the function $f_M(m)$, which represents the logarithmic frequency shift as a function of the moisture content in (9) and (10). Little can be said about this function from the data in Table 5. Therefore we choose a form that would yield the simplest algebra

$$f_M(m) = c_m + \log m \qquad (26)$$

whose best fitted curve is shown in Figure 11. The curve in this Figure corresponds to $c_m = -0.684$, if m is in percent and the frequency is in Hertz.

Combining (9), (10), and (24) to (26) yields the final functional form

$$\varepsilon^* = \varepsilon_\infty + \varepsilon_0 c \left(\frac{m}{\omega}\right)^{-\gamma} \qquad (27)$$

in which c is a complex coefficient defined as
$c = 10^{-\gamma(f_T(T)+c_m)}(10^{c_1} - i\,10^{c_2})$.

Substituting (23) into (27) gives the general form of the dielectric profile of pressboard, most conveniently written as

$$\varepsilon^*(\xi) = \varepsilon_\infty +$$

$$\varepsilon_0 G \left[\frac{1}{\omega}\left(1 - \frac{C}{2} + C\sum_{n=1,\text{odd}}^{\infty} \frac{4}{\pi n}e^{-Dtk_n^2}\sin k_n\xi\right)\right]^{-\gamma} \qquad (28)$$

where $G = c(A + B/2)^{-\gamma}$ and $C = 2B/(2A + B)$. The range of physical values for C, *i.e.* values for which the moisture content is non-negative, is $C \in [-2, 2]$.

The dielectric profile is fully specified by the three parameters G, C, and Dt. If these parameters are found by an estimation method, then the dielectric profile of the pressboard, and therefore its moisture profile, are fully specified. The first of these coefficients is complex (G), but the other two $(C$ and $Dt)$ are real, for a total of four degrees of freedom. In separating the real and imaginary parts of (28) it is found that data from three wavelengths is needed to solve for the unknown parameters of this function [13, Sect. 4.1.2].

Relating the gain/phase response of a sensor to the medium above it, described by (28), is more complicated than before, when the variation in the complex permittivity of the medium was described by a stair-step function. Now ε^* is a function of position and this must be accounted for in the mathematical model. However, since

the only three parameters being estimated are those in (28), the spatial variation of ε^* may be arbitrarily closely approximated by a stair-step function with a large number of intervals, and therefore the previously developed algorithms for calculating the gain and phase are still useful.

5. PROFILE MEASUREMENTS
5.1. EXPERIMENTAL SETUP

In order to measure moisture profiles in pressboard, the sample had to be placed in a controlled environment, which allowed moisture to diffuse in and out of the pressboard from one surface. The other surface of the sample was sealed by the sensor itself. For this purpose the experimental setup shown in Figure 18 was created. The stainless steel chamber can be filled with transformer oil, whose moisture content can be varied by bubbling wet or dry nitrogen through it, or the chamber can remain full of air with controlled pressure and humidity, as was done in the experiments presented there. Since intimate contact between the pressboard and the sensor needs to be maintained, the sample has to be tightly squeezed from both sides. The teflon and aluminum layers serve this purpose, while at the same time allowing mass-transfer processes to occur at $\xi = 0$ through a multitude of holes. They are attached to the aluminum base with insulating nylon bolts.
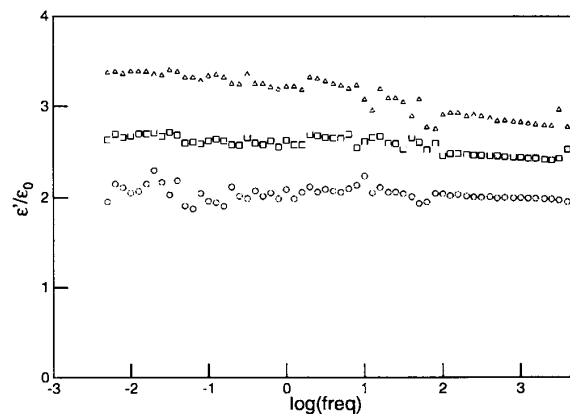

Figure 19.

Permittivity of polymer structure as calculated from every wavelength of the three-wavelength sensor. $\triangle \lambda = 5$, $\square \lambda = 2.5$, $\bigcirc \lambda = 1$ mm.

5.2. POLYMERS

Before using the three-wavelength sensor to measure profiles in pressboard, we decided to test it on polymers. We substituted the pressboard layer in Figure 18 with three layers of polymers, listed in Table 9, and took a full frequency scan.

Table 9.

Layer structure for polymer experiment. Permittivity data is taken from [18] at 1 kHz and room temperature.

Layer	Material	Thickness [mm]	Permittivity
0	PMMA	12.3	3.12 ε_0
1	LDPE	0.066	2.26 ε_0
2	HDPE	0.028	2.26 ε_0
3	Parylene	0.005	2.70 ε_0

The phase angle remained close to zero for the entire frequency range, indicating that the conductivities of these materials are too low to make a contribution. Using the one-dimensional parameter estimation routine (Section 4.1) we estimated the properties of the polymer layer for every wavelength independently, in order to obtain a qualitative picture of the permittivity distribution, shown for each wavelength in Figure 19. Only ε' data is shown because the conductivity was too low to measure.

The longest wavelength in Figure 19 measured the highest value of the permittivity, indicating that the topmost Plexiglas[TM] layer had a higher permittivity than the other two materials, which is consistent with the permittivities of these plastics, listed in Table 9 [18]. The effective depth of penetration of an interdigitated sensor is typically of order $\lambda/4$ [1,4]. The reach of the shortest wavelength, $\lambda_3 = 1$ mm (Table 6), is therefore ~ 0.25 mm. The combined width of layers 1 and 2 is < 0.1 mm, which means that all three wavelengths reach the Plexiglas layer. The thickness of the Plexiglas layer is $\sim 10\times$ larger than the depth of penetration of the longest wavelength, and may be assumed to be infinite.

The measurement in Figure 19 is consistent with the values of the permittivity of the materials listed in Table 9. The Plexiglas layer shows some dispersion, since the permittivities increase with lower frequencies. The shortest wavelength displays the least pronounced dependence on ω, because it is least sensitive to the properties of the Plexiglas.

The data in Figure 19 seems to be more noisy than other dielectric spectra presented so far. This is due to the fact that the phase angle of the response is close to zero and the noise compensating influence of having two pieces of data per measurement is absent. The inversion algorithms can only rely on magnitude data, which has a typical measurement tolerance of 0.5 dB, corresponding to 6% noise.

When we applied the root-finding multidimensional parameter estimation algorithm (Section 4.3.1) to the data at 1 kHz, poor results were obtained. Although the method worked correctly, the results are unrealistic,

because the spatial dielectric profile seen by every wavelength is not sufficiently distinct. All three wavelengths were primarily influenced by the Plexiglas layer and as a result the signal-to-noise ratio of the method with respect to the other two layers is quite low. For good results the unknown layers' thicknesses should be of the same order of magnitude as the depths of penetration of the different wavelengths, so that the shortest wavelength is most sensitive to the closest layer, *etc.* Therefore the three-wavelength sensor should work best on 0.5 to 2 mm thick layers.

For the polymer experiment described in this section, the inversion algorithm that yielded the most information was the one-dimensional parameter estimation.

5.3. OIL-IMPREGNATED PAPER

Preliminary measurements with the three-wavelength sensor on EHV-Weidmann HIVAL pressboard exhibited inconsistency in the values of the permittivity between the three wavelengths and the known properties of pressboard (from Section 2). We realized that because of the textured surface of that kind of pressboard, an effective oil layer was formed between the pressboard surface and the Parylene coating. Although such a layer can easily be included in the model, it would introduce another unknown and make the measurements less sensitive to the properties of the pressboard instead.

This is why we chose to conduct our profile measurements with Crocker[TM] paper, which is a very similar cellulose insulating material with much the same applications as pressboard. The Crocker paper samples had a very smooth surface, which eliminated the problem of the extra oil layer. In addition to that, the smooth surface of the paper made it possible to stack many layers without worrying about empty space left between the plies. The Crocker paper sample, with which we conducted the experiments discussed in this Section, was 0.25 mm thick. Sixteen plies of paper added up to a total thickness of 4 mm, thus making the measurement sufficiently independent of the layers on the other side of the paper. The paper was impregnated with Shell Diala A transformer oil.

First we examined the oil-impregnated Crocker paper sample with the parallel-plate sensor, described in detail in Section 2.1. The dielectric spectrum of the sample was taken at room temperature. It is shown in Figure 20. This Figure is included mainly as a 'sanity check' reference for all subsequent measurements with the three-wavelength sensor on Crocker paper.

The dielectric spectrum of the Crocker paper sample in Figure 20 differs from the spectrum of HIVAL pressboard (Figure 9) in that in addition to the dominant loss peak,
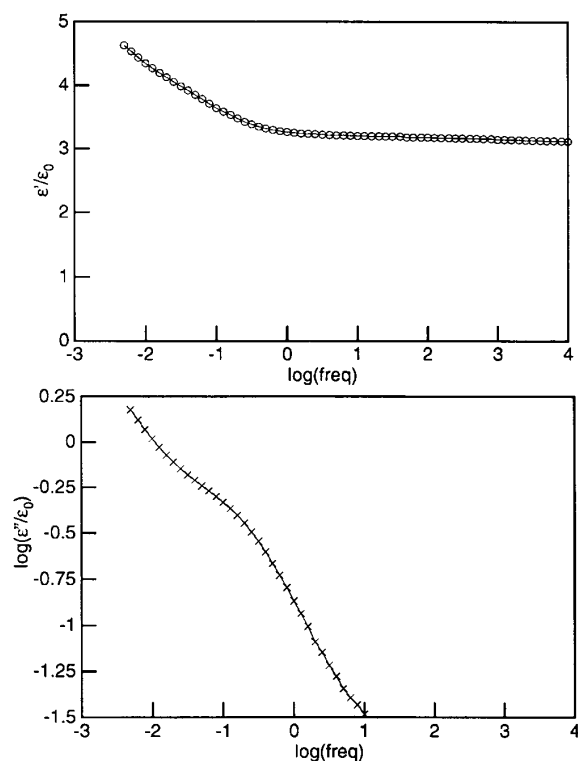
Figure 20.

Dielectric spectrum of oil-impregnated 0.25 mm Crocker paper at room temperature using the parallel-plate sensor.

Figure 21.

Dielectric spectra taken with the three-wavelength sensor on Crocker paper. $\triangle$ λ = 5, $\square$ λ = 2.5, $\bigcirc$ λ = 1 mm.

which occurs at frequencies < 0.005 Hz and is present in both materials, another loss peak is visible at ~ 0.2 Hz. This minor peak is responsible for the curved shape of the ϵ'' plot between 0.01 and 0.1 Hz.

The first set of measurements with the three-wavelength sensor on the sixteen-ply Crocker paper structure was conducted in air immediately after the oil-impregnated samples had been dried under vacuum. The results from the one-dimensional parameter estimation algorithm, applied to the data from all three wavelengths with the assumption of a single unknown homogeneous layer, are shown in Figure 21. The shortest wavelength measured the highest value of ϵ'', suggesting that the layer closest to the sensor is more conducting as compared to the bulk of the paper.

This high conductivity near the surface of the sensor may be attributed to the absorption in the paper of moisture which had been adsorbed on the sensor surface.

We also applied the above root-finding multidimensional search to the data at 0.01 Hz. The results are
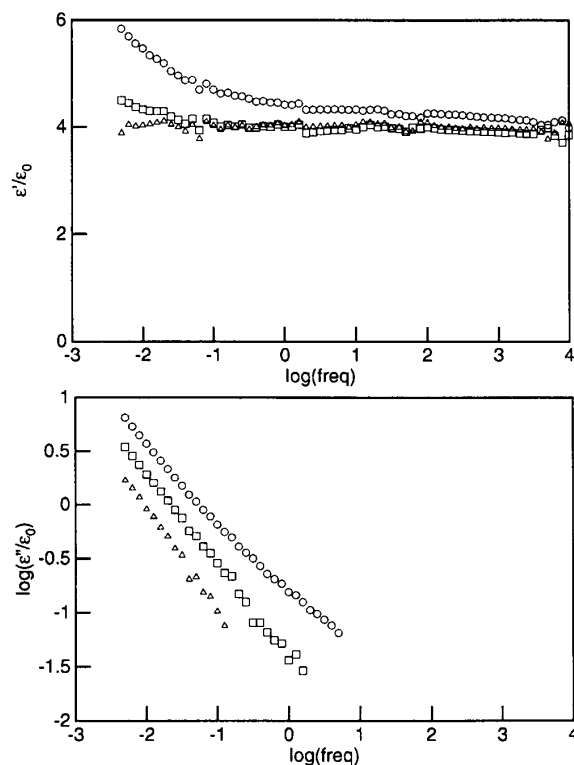
shown in Table 10. The values of the permittivities are in the order expected from looking at Figure 21, *i.e.* layer 2 had the highest value. It is disturbing to see a negative value of the conductivity of layer 1. This phenomenon has a simple explanation. The dielectric relaxation time (in s) of layer 2, which is closest to the sensor, is

$$\tau_e = \frac{\epsilon}{\sigma} = \frac{4.79 \times 10^{-11}}{2.32 \times 10^{-12}} = 20.6 \qquad (29)$$

corresponding to a relaxation frequency (in Hz) of

$$f_e = \frac{1}{2\pi\tau_e} = 0.0077 \qquad (30)$$

This estimation was based on a layer 2 thickness of d_2 = 0.25 mm. The highly conducting interfacial zone may be much thinner and more highly conducting than these estimates, corresponding to even higher values of the relaxation frequency. This means that at 0.01 Hz the electric fields are shielded from the rest of the paper and the parameter estimation for layers 0 and 1 becomes a victim to a low signal-to-noise ratio.
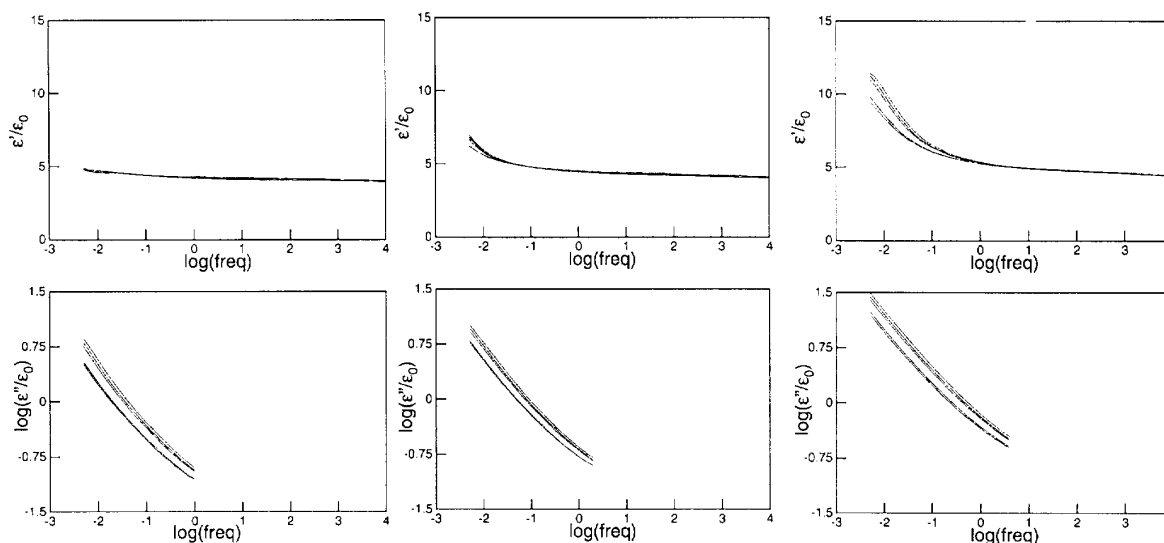
Figure 22.

Dielectric spectra of oil-impregnated Crocker paper drying under vacuum, taken with all three wave-lengths. The five spectra, in descending order, correspond to frequency scans taken at 1, 6, 12, 57, and 86 h after the application of the vacuum.

Table 10.

Results from applying the root-finding multidi-mensional algorithm to Crocker paper data at 0.01 Hz.

Layer	Thickness mm	Permittivity ε_0	Conductivity S
0	∞	1.55	7.49×10^{-13}
1	0.25	3.29	-1.50×10^{-12}
2	0.25	5.41	2.32×10^{-12}

After that, vacuum was applied to the chamber and continuous frequency scans were taken every hour, in or-der to monitor the drying process. Figure 22 shows the results from the application of one-dimensional param-eter estimation to the data from each individual wave-length. The Figure shows the dielectric spectra mea-sured by each wavelength independently at five specific times: 1, 6, 12, 57, and 86 h after the application of vac-uum. The dielectric spectra in this Figure shift to the left with time, indicating by the decrease in conductivity that moisture is leaving the paper.

The application of the multidimensional search to the same data that yielded the results in Figure 22 at 0.01 Hz produced the results listed in Table 11. The table lists the estimated dielectric properties of the layer closest to the sensor (layer 2), showing the low frequency disper-sion by its enhanced permittivity. These results are in agreement with the trends seen in Figure 22 and provide a quantitative measure of the decrease in conductivity associated with the drying. As already discussed, this

conducting layer greatly reduced the sensitivity of this estimation to the properties of the other two layers.

Table 11.

Results of applying the multidimensional param-eter estimation algorithm to data at 0.01 Hz taken after the application of vacuum to oil-impregnated Crocker Paper at time $t = 0$. The tabulated values are for the Crocker paper layer closest to the three-wavelength sensor (layer 2).

Time [h]	ε_2	σ_2
1	$10.2\ \varepsilon_0$	1.41×10^{-11}
6	$9.66\varepsilon_0$	1.29×10^{-11}
12	$9.57\varepsilon_0$	1.23×10^{-11}
57	$9.48\varepsilon_0$	9.49×10^{-12}
86	$8.45\varepsilon_0$	6.24×10^{-12}

6. CONCLUSIONS
6.1. UNIVERSAL SPECTRUM

THE importance of the 'universal' dielectric spectrum presented in Section 2 is that a relationship may be developed between the dielectric properties and one or more physical properties of a material. While Section 2 did present one such universal spectrum, it also estab-lished a methodology of obtaining such spectra for a ma-terial. The measurement method with the parallel-plate sensor can be used on any material.

While taking the dielectrometry measurements with a parallel-plate sensor, it is important that the material is

homogeneous. For example, our work showed that for moisture to reach a uniform concentration in a 1 mm thick pressboard sample, five days at 50°C were needed.

A method of combining the data from all dielectric spectra was discussed in Section 2.3, which allowed all thirty-five measurements to be merged into a single universal curve. This process resulted in a relationship between the manner in which the individual spectra are moved in frequency in order to form a single curve and the physical parameters being varied. This relationship could later be used in the opposite direction to obtain moisture content or temperature information from a dielectric measurement.

For oil-impregnated pressboard the dielectric spectra were shifted horizontally with frequency on a logarithmic scale, the shift being a function of the two physical parameters under consideration, temperature and moisture content. An important conclusion of the analysis of this function was that the effects due to variations in each of these two physical parameters were independent of each other (see (9), (10)).

The limited range of temperature variation, $\sim$ 13% on an absolute temperature scale, made it difficult to find the exact functional form of the relationship describing the frequency shift due to temperature, although an Arrhenius dependence fit the data quite well. Future work should include testing a wider temperature range.

The relationship describing the frequency shift due to moisture was difficult to establish for a different reason. The calibration moisture measurement with the vaporizer has a wide error margin. Therefore many more data points in Figure 11 are necessary in order to establish the functional form with confidence. When it is considered that performing measurements on one pressboard sample takes a week to allow for the conditioning transient to die away, it is clear why only seven data points are present in that Figure. In order to find the universal dielectric spectrum of a material together with its accompanying functions, it is necessary to perform many more tests than we were able to do. However, we did establish a procedure that can be followed to obtain such universal spectra.

6.2. PARAMETER ESTIMATION

Parameter estimation is the process of calculating the complex permittivities of the materials above an interdigitated sensor from measured gain-phase data. It is the reverse of finding the gain phase response of a sensor if the material above it is known, often referred to as the forward problem. The forward problem is solved in [1] and [2] for the case of a number of homogeneous layers of constant complex permittivity. In other words, the

solution presented in that section is only applicable for cases where the complex permittivity profile is a stair-step function of the spatial variable x. Other spatial profiles can be found as solutions to Poisson's equation with spatially varying complex permittivity.

Parameter estimation is performed numerically, because it is impossible to find closed-form solutions to the reverse problem. It can be implemented as iterative root-finding techniques or optimization techniques. The simplest case is the one-dimensional search, where the complex permittivity of only one parameter is unknown.

Flexible sensors with different spatial wavelengths may be used to extract information about the spatial profile of the dielectric properties of a material by combining the results of several sensors of different spatial wavelengths.

In addition to the previously developed marching approach [15], we have developed two other methods of processing the data from measurements with more than one wavelength: the multidimensional search, and the multidimensional search with an assumed profile function. The marching approach is simpler and more reliable and it is only valid when there is one unknown inhomogeneous layer extending to infinity, but it is not applicable to arbitrary structures, since the thicknesses of the layers are prescribed by the sensor wavelengths. Both the marching approach and the multidimensional search approximate the profile with a stair-step distribution. The multidimensional search may be done either as a root-finding problem, in which case exact solutions are sought, or as an optimization problem in which case the minimum of an error function is sought. The second option allows for including data from more wavelengths than there are unknowns.

The multidimensional search with an assumed profile function attempts to include in the estimation algorithm some knowledge of the physics of moisture diffusion, by using a smooth function to represent the variation of the dielectric properties of the pressboard across its thickness. It is a root-finding problem where the unknowns are some parameters of this assumed function.

All of these methods need refinement, although we have successfully used them in some applications. One of the major difficulties is that because the forward problem is very nonlinear, the multidimensional algorithms may become unstable or otherwise fail to find a root if the initial guess is too far from the solution. This is why it is very important to start with a good first guess to a multidimensional estimation problem, perhaps from applying the one-dimensional algorithm to every individual wavelength first.

Which of these parameter estimation routines is preferred depends on the characteristics of the particular problem.

6.3. MOISTURE PROFILES

We have used the ideas about measuring dielectric profiles, developed in Sections 3 and 4, on measurements with the three-wavelength sensor on polymers and oil-impregnated paper. One of the obstacles in measuring spatial profiles by probing the material from only one surface is that a highly conducting layer near the surface will limit the electric fields from penetrating into the material and reduce the measurement's sensitivity to the bulk dielectric properties.

Altogether the experiments confirm the feasibility of the method of calculating dielectric profiles. Depending on the application a choice must be made about the spatial wavelengths of the interdigitated sensors, the frequency range, and the most appropriate parameter estimation algorithm, so that the greatest amount of information about the material properties is extracted from the measurements.

Future work should include more diagnostic profile measurements with polymers or other well known materials, selecting their thicknesses in a way that would make the estimation methods sensitive to all layers. Slightly conducting polymers would be a good choice, because this would test the methods under more general conditions than very insulating materials could. More experiments on measuring moisture dynamic processes in pressboard with the three-wavelength sensor are also needed. When confidence is gained in the use of the simpler parameter estimation methods, the method of using an assumed profile function, presented in Section 4.4, should be further studied.

ACKNOWLEDGMENT

REFERENCES

[1] M. C. Zaretsky, *Parameter Estimation Using Microdielectrometry with Application to Transformer Monitoring*, p. 88, PhD thesis, Department of Electrical Engineering and Computer Science, Massachusetts Institute of Technology, Cambridge, MA, November 1987.

[2] M. C. Zaretsky, L. Mouayad, J. R. Melcher, "Continuum Properties from Interdigital Electrode Dielectrometry", IEEE Transactions on Electrical Insulation, Vol. 23, No. 6, pp. 897–917, December 1988.

[3] P. Li, *Low Frequency, Millimeter Wavelength, Interdigital Dielectrometry of Insulating Media in a Transformer Environment*, LEES Technical Report TR-87-005, Massachusetts Institute of Technology, May, 1987.

[4] P. A. von Guggenberg, *Applications of Interdigital Dielectrometry to Moisture and Double Layer Measurements in Transformer Insulation*, PhD thesis, Section 6.3. Department of Electrical Engineering and Computer Science, Massachusetts Institute of Technology, Cambridge, MA, June 1993.

[5] K. Miners, "Particles and Moisture Effect on Dielectric Strength of Transformer Oil Using VDE Electrodes", IEEE Transactions on Power Apparatus and Systems, Vol. 101, No. 3, pp. 751–756, March, 1982.

[6] S. R. Lindgren, A. P. Washabaugh, P. A. von Guggenberg, M. Zahn, M. Brubaker, J. K. Nelson, "Temperature and Moisture Transient Effects on Flow Electrification in Power Transformers", 1992 CIGRE Meeting, Paris, France.

[7] W. Kennedy, "Resistivity of Oil and Pressboard Insulation and their Effect on Transformer Design", EPRI Proceedings: Static Electrification in Power Transformers, EPRI TR-102480, Project 1499-99, pp. 1-4-1 to 1-4-13, June, 1993.

[8] A. K. Jonscher, *Dielectric Relaxation in Solids*, Chelsea Dielectrics Press, London, 1983.

[9] T. V. Oommen, "Moisture Equilibrium Charts for Transformer Drying Practice", IEEE Transactions on Power Apparatus and Systems, Vol. 103, pp. 3063–3067, October, 1984.

[10] T. V. Oommen, "Moisture Migration between Paper and Oil in Transformers", EPRI Proceedings: Static Electrification in Power Transformers, EPRI TR-102480, Project 1499-99, pp. 1-3-1 to 1-3-7, June, 1993.

[11] B. Nettelblad, "Effect of Moisture Content on the Dielectric Properties of Cellulose", Paper 8.9, NORD-IS 92, 1992.

[12] U. Gäfvert, B. Nettelblad, "Measurement Techniques for Dielectric Response Characterization at Low Frequencies", Paper 7.1, NORD-IS 92, 1992

[13] Y. K. Sheiretov, *Dielectrometry Measurements of Moisture Dynamics in Oil-Impregnated Pressboard*, Master's thesis, Department of Electrical Engineering and Computer Science, Massachusetts Institute of Technology, Cambridge, MA, May 1994.

[14] Y. Sheiretov, M. Zahn, "A Study of the Temperature and Moisture Dependent Dielectric Properties of Oil-Impregnated Pressboard", 1993 Conference on Electrical Insulation and Dielectric Phenomena, Pocono Manor, PA, October 17–20, 1993.

[15] P. A. von Guggenberg, M. C. Zaretsky, "Estimation of One-Dimensional Complex Permittivity Profiles: A Feasibility Study", Journal of Electrostatics, Vol. 34, No. 2-3, pp. 263–277, 1995.

[16] W. H. Press, B. P. Flannery, S. A. Teukolsky, W. T. Vetterling, *Numerical Recipes; The Art of Scientific Computing*, Cambridge University Press, 1986.

[17] F. B. Hildebrand, *Advanced Calculus for Applications*, 2nd Edition, Prentice-Hall, Inc., Englewood Cliffs, NJ, 1976.

[18] *CRC Handbook of Chemistry and Physics*, 61st edition, CRC Press, Inc., Boca Raton, FL, 33431, 1981.

[19] Y. Sheiretov, M. Zahn, "Dielectrometry Measurements of Moisture Dynamics in Oil-Impregnated Pressboard", 1994 IEEE International Symposium on Electrical Insulation, Pittsburgh, PA, June 5–8, 1994.

[20] Y. Sheiretov, M. Zahn, "Dielectrometry Measurements of Spatial Moisture Profiles in Oil-Impregnated Pressboard", 4th International Conference on Properties and Applications of Dielectric Materials, The University of Queensland, Brisbane, Australia, July 3–6, 1994.